

Experimental test of the self-organized criticality of vortices in superconductors

V. K. Vlasko-Vlasov,¹ U. Welp,¹ V. Metlushko,² and G. W. Crabtree¹

¹Argonne National Laboratory, Argonne, Illinois 60439, USA

²University of Illinois, DECE, Chicago, Illinois 60607, USA

(Received 2 February 2004; published 6 April 2004)

Magneto-optical studies of the vortex dynamics in Nb films reveal stochastic jumps of flux bundles forming a rough penetration front. The scaling analysis of the width, correlation function, and the length of flux profiles behind the front retrieves the roughness exponents and Housdorff dimension characterizing the self-organized critical state. The exponents correspond to (1+1)-dimensional nonlinear diffusion in systems with quenched disorder and long-range correlations. The power spectra of the profiles confirm the self-affine character of the dynamically formed critical state.

DOI: 10.1103/PhysRevB.69.140504

PACS number(s): 74.25.Qt, 05.45.-a, 05.65.+b, 74.78.-w

The self-organized criticality¹ (SOC) accompanied by the pattern formation is considered to be a general feature of many physical systems with disorder. Examples are superconducting vortices, granular media, charge-density waves, earthquakes, dislocations, polymers, magnetic domain walls, growing crystals, wetting, and burning phenomena.² The dynamics of these complex systems is characterized by a hierarchy of spatial and temporal scales described by power laws within several decades of sizes and times.³ Such a *power-law* behavior is presently accepted as the main indication of SOC. The values of appropriate exponents turn out to be universal and refer the system to one of the universality classes associated with relevant dynamical equations.

There were several experimental attempts to prove the SOC of vortices entering type-II superconductors in the shape of flux jumps, but the situation is still ambiguous. Direct measurements of the flux jump distributions,⁴⁻⁷ dB/dt spectra,^{5,8} and features of the flux relaxation^{9,10} in both low- and high- T_c materials so far did not result in a clear and consistent picture. In some cases the SOC-type power law for the jump distribution function was reported over ~ 2 decades of jump sizes s .^{5,8,10} In other cases such a trend was not observed⁴ or observed in limited ranges of s and narrow temperature windows^{6,7} leading to a conclusion of non-SOC dynamics. Good fits of the relaxation data using formulas that account for SOC-like vortex avalanches⁹ caused reasonable doubts as it turned out that SOC features cannot be retrieved from the classical relaxation measurements.¹¹ Also, it was suggested that under some conditions the relaxation through avalanches of many sizes does not mean the existence of SOC.¹²

An interesting analysis of a possible SOC dynamics of vortices was proposed recently in Ref. 13 based on well-established scaling concepts used for studies of rough interfaces in stochastic systems.² It was reported in Ref. 13 that the kinetic roughening of the flux penetration front in a thin yttrium barium copper oxide (YBCO) film exhibits the dynamical scaling with well-defined self-affine exponents. Moreover, a change in the growth exponent was noticed and associated with different scaling regimes dominating at different length scales. The observed behavior was compared to the kinetic roughening in burning paper that fits with the SOC scenario for the nonlinear diffusion.

Inspired by this work we performed a magneto-optical study of rough flux fronts in low- T_c Nb films. However, we started from the idea that there is an *important difference* between growth and burning phenomena and the superconducting critical state dynamics. If in the former two the structure behind the front is fixed, the evolution of the critical state behind the penetration front in a superconductor does not cease. Therefore, we analyzed not only the flux front but also flux profiles behind it. We directly, and in a real time, observed intermittent vortex avalanches in the samples changing to a smooth flux entry at larger temperatures. In addition to the statistical analysis of the width and correlation function of the flux profiles we determined their Housdorff dimension and found power laws with exponents characteristic for nonlinear diffusive systems with long-range correlated noise. The analysis of power spectra of the profiles confirmed their self-affine nature and global scaling behavior suggesting the universal SOC in the vortex system in some temperature range below T_c .

We studied 100 nm thick Nb films with $T_c = 8.5$ K grown by dc magnetron sputtering on Si substrates. A magneto-optical technique utilizing garnet indicators¹⁴ was used to image magnetic-flux patterns from 3.5 K to T_c . The field was applied perpendicular to the film and spatial variations of the flux density were observed in the polarized light as changes in the local image intensity. The technique allowed for real time observations of the flux dynamics and measurements of the field maps using a 16 bit 1024×1024 pixel CCD array. From these maps we obtained profiles of the constant flux density and analyzed their width, length, correlation functions, and power spectra. The field ramp was very slow (1 Oe/min) in order to reveal saturated scaling relations characterizing geometrical features of the flux diffusion in random potential.

At T above ~ 6.5 K the flux entry and $B_z(r) = \text{const}$ profiles were smooth and did not show a developed fractal structure. Below 4.2 K large catastrophic thermomagnetic avalanches similar to those reported in Ref. 15 strongly disturbed the flux patterns. However, at intermediate temperatures a remarkable intermittent dynamics of varying size flux jumps was clearly seen reminiscent of the popular scenario of sand avalanches. It showed up as fast flickering of the local flux density during the slow field ramp. The result-

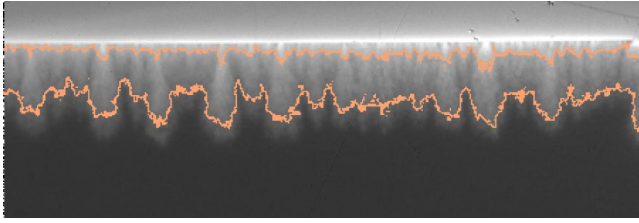


FIG. 1. (Color online) Flux pattern and profiles $B_z=20$ G (near the sample edge) and $B_z=2.6$ G (near the flux front) at $H_a=6$ Oe. $T=4.5$ K. The local intensity is proportional to the B_z value.

ing flux pattern had an average gradient perpendicular to the film edge and revealed inhomogeneities and rough B_z profiles as shown in Fig. 1. Below we present a statistical analysis of these profiles.

For a self-affine surface in stochastic systems, described as a function $h(\mathbf{r}, t)$ of coordinates \mathbf{r} and time t , the following Family-Vicsek scaling relations are expected.² The *global width* W of the surface defining square deviations from the average position is represented as

$$W(L, t) = \langle \langle [h(\mathbf{r}, t) - \langle h(t) \rangle]^2 \rangle \rangle^{1/2} = t^{\alpha/z} g(L/t^{1/z}), \quad (1)$$

$$g(u) \sim \begin{cases} u^\alpha & \text{if } u \leq 1 \Rightarrow W \sim L^\alpha & \text{if } t \geq L^z \\ \text{const} & \text{if } u \geq 1 \Rightarrow W \sim t^{\alpha/z} & \text{if } t \leq L^z. \end{cases} \quad (2)$$

Here $\langle \dots \rangle_L$ and $\langle \dots \rangle$ are averaging over the system size L and over realizations, respectively, α is the *roughness* exponent (in most cases, identical to the *Hurst* exponent), z is the *dynamical* exponent, and the ratio α/z is the *growth* exponent β . These exponents characterize the *universality class* of a nonlinear diffusion model capturing the physics of the surface evolution. In windows of a smaller size ℓ the *local width* $w(\ell, t)$, which is usually measured in the experiment, has the same scaling, Eqs. (1) and (2), with L changed for ℓ . However, in many systems the roughness exponent in the scaling function $g(u)$ acquires a local value α_ℓ different from α (*anomalous scaling*¹⁶ changing the universality class) so that

$$w(\ell, t) \sim \begin{cases} \ell^{\alpha_\ell} t^{(\alpha - \alpha_\ell)/z} & \text{if } t \geq \ell^z \Rightarrow \ell^{\alpha_\ell} L^{(\alpha - \alpha_\ell)} & \text{at } t \sim L^z \\ t^{\alpha/z} & \text{if } t \leq \ell^z \text{ [as in Eq. (2)].} \end{cases} \quad (3)$$

The same scaling (3) is expected for the two-point *correlation function*:

$$C(\ell, t) = \langle \langle [h(\mathbf{r} + \ell, t) - h(\mathbf{r}, t)]^2 \rangle \rangle^{1/2}. \quad (4)$$

Due to the same form of the scaling function it is hard to reveal the anomalous behavior ($\alpha_\ell \neq \alpha$) from w and C . However, it can be done using the *power spectrum* of the surface which presents the square Fourier components of $h(\mathbf{r}, t)$: $S(k, t) = \langle h(\mathbf{k}, t) h(-\mathbf{k}, t) \rangle$. In the self-affine case it scales as

$$S(\mathbf{k}, t) \sim k^{-(2\alpha+d)} s(kt^{1/z}), \quad (5)$$

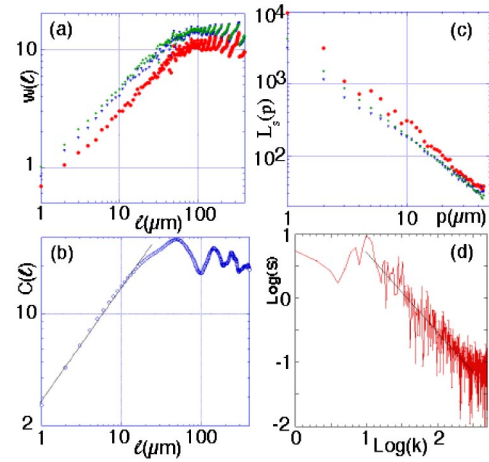


FIG. 2. (Color online) (a) The width w of $B_z=\text{const}$ profiles ($B_z=2.6, 5.4$, and 11.4 G from top to bottom) and (b) the correlation function C of a profile $B_z=5.4$ G at $H_a=8$ Oe. (c) Profile length L_s measured in pixels of different size p at $B_z=1.4, 2.6$, and 11.4 G (from top to bottom) and (d) Power spectrum $S(k)$ for the profile $B_z=5.4$ G at $H_a=6.1$ Oe. $T=4.5$ K.

$$s(u) \sim \begin{cases} u^{2\alpha+d} & \text{if } u \leq 1 \Rightarrow S(k) \sim t^{(2\alpha+d)/z} & \text{if } k \leq 1/t^{1/z} \\ \text{const} & \text{if } u \geq 1 \Rightarrow S(k) \sim k^{-(2\alpha+d)} & \text{if } k \geq 1/t^{1/z}, \end{cases} \quad (6)$$

where d is the dimension of the reference surface (for our flux profiles $d=1$). The same scaling is obtained for the frequency spectra $S(f)$ [k is changed for f in Eq. (6)]. For the anomalous scaling a new $s(u)$ form appears with a third *spectral* exponent α_s :¹⁷

$$s(u) \sim \begin{cases} u^{2\alpha+d} & \text{if } u \leq 1 \\ u^{2(\alpha - \alpha_s)} & \text{if } u \geq 1. \end{cases} \quad (7)$$

If $\alpha_s < 1$, $\alpha_s = \alpha_\ell$ and either $\alpha_\ell \neq \alpha$ (local \neq global) or $\alpha_\ell = \alpha$ [local=global, Eq. (6)]. In the case $\alpha_s > 1$, $\alpha_\ell = 1$ and either $\alpha_s = \alpha$ (superroughening) or $\alpha_s \neq \alpha$ (new class).

The scaling exponents have a direct link to the Hausdorff dimension of the rough surface determined as²

$$D = \lim_{p \rightarrow 0} [\ln N / \ln(1/p)]. \quad (8)$$

Here N is a number of elements of size p required to cover the surface (box counting method). For the self-affine surfaces

$$D = d + 1 - \alpha. \quad (9)$$

Figure 2(a) shows the local width $w(\ell)$ of B_z profiles for a flux pattern formed at $T=4.5$ K in external field $H_a=8$ Oe. The profiles are acquired near the middle of the edge in a $\sim 4 \times 4$ mm² film. Increasing B_z corresponds to profiles taken closer to the sample edge, where $B_z \gg H_a$ due to the shape effect. At smaller ℓ the log-log plot reveals a good power-law shape of $w(\ell)$ that transits to oscillations around a saturation level at larger ℓ . Similar small scale power law and the change in slope at larger scales were reported for $w(\ell)$ in YBCO.¹³ Unlike in Ref. 13 we refer this change to the artifact of treatment in a finite-size win-

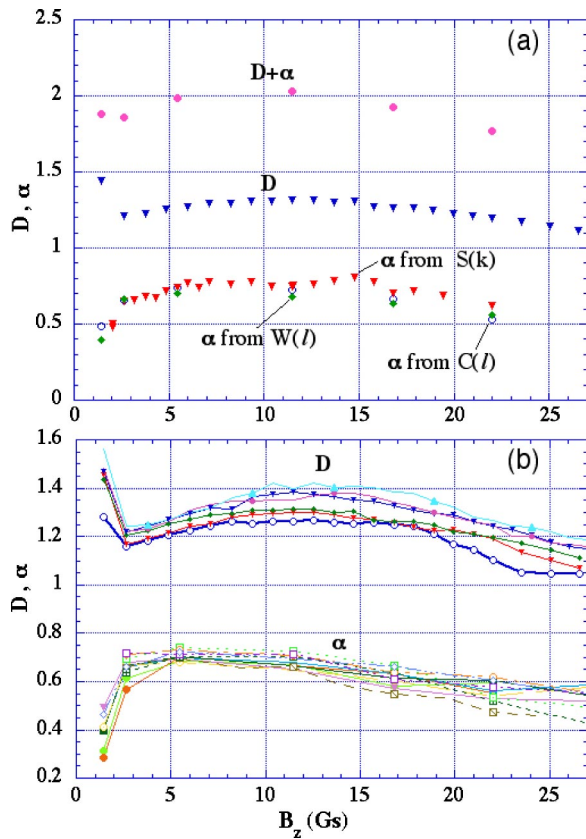


FIG. 3. (Color online) (a) Exponents retrieved from the profile width $w(\ell)$, correlation function $C(\ell)$, and power spectra $S(k)$, and the Housdorff dimension from the profile length $L_s(p)$ at different B_z levels ($H_a = 6.1$ Oe, $T = 4.5$ K). Also the sum $D + \alpha$ is shown. (b) Exponents at different B_z levels for flux patterns measured in external fields of 4, 5.2, 6.1, 7.5, 8.2, and 9 Oe.

down \mathcal{L} determining the $w(\ell)$ oscillations at $\ell > 0.1\mathcal{L}$. The correlation function $C(\ell)$ follows the same behavior as illustrated in Fig. 2(b). We retrieved the roughness exponent α_ℓ from the initial slope of $w(\ell)$ and $C(\ell)$ and plotted it as a function of B_z in Fig. 3(a). It has an unexpected nonmonotonic behavior reaching maximum $\alpha \sim 0.7$ (close to 0.64 reported in Refs. 13) at some distance behind the penetration front ($B_z \sim 0$) and decreasing towards the edge (largest B_z). This reduction of the roughness could be due to the alignment of the current flow by the edge. The length of the profiles measured in different pixel sizes, $L_s(p)$, is presented in Fig. 2(c). It shows a distinct power behavior allowing to estimate the Housdorff dimension D which is plotted as a function of B_z of the profiles in Fig. 3(a). This function reveals changes complementary to those of α . D goes from maximum at the front ($B_z \sim 0$) to a minimum at some distance behind it, then increases and reduces again at the sample edge (max B_z). Interestingly, the sum of $D + \alpha$ is ~ 2 as it is expected from Eq. (9) with $d = 1$. Figure 3(b) shows all the exponents for a number of flux patterns formed at different external fields. Profiles with the same B_z are obtained here at different depth from the edge. Remarkably, they all overlap in a very consistent manner which may indicate to a global scaling in the vortex system. To confirm

this we analyzed the power spectra of the profiles as prescribed in Ref. 16.

Figure 2(d) presents the power spectra $[S(k)]^{1/2}$ of the flux profiles at different B_z levels. They are symmetric with respect to the middle of the $k = 1-1024$ window and are shown only up to $k = 512$. The spectra are noisy, which is typical for systems with quenched disorder.^{15,18} The points at $\ln k < 1$ corresponding to distances > 100 pixels (1 pixel = 1 μm) are shifted from the main trend due to the finite-size effect and are not used in the analysis. At $\ln k \sim 2.7$ ($k \sim 512$) $S(k)$ in a log-log scale is also turning from the linear behavior. Therefore we used a linear fit in a shorter range, $1 < \ln k < 2.5$, to determine the exponent which in our long-time case [bottom formula in Eq. (7)] should be given by $S(k) \sim k^{-(2\alpha_s+1)}$. The fitting values of α_s for profiles at different B_z are shown in Fig. 3(a). They are remarkably close to the roughness exponents extracted from C and w confirming that $\alpha_s = \alpha_\ell = \alpha$. So the scaling is global and the magnetic-flux structure is self-affine.

The electrodynamics of superconductors representing the flux motion is described by the nonlinear diffusion scenario following from the Maxwell equations.¹⁹ However, in order to study the fractal details of the flux patterns one has to explicitly account for disorder terms. This results in a Langevin-type growth equation and defines a model generating characteristic exponents of the critical state.² Below we discuss some models that yield roughness exponents close to our experimental values.

An “*anomalously large*” value of α (> 0.63) was obtained in many fractal experiments, including wetting of porous media, propagation of combustion fronts, growth of cell colonies, polycrystalline and epitaxial film growth, colloidal deposition, erosion, and other processes (see in Ref. 2). These phenomena may be related to the modified Kardar-Parisi-Zhang (KPZ) universality class. A regular KPZ equation with uncorrelated disorder predicts $\alpha = 1/2$ for (1+1)-dimensional interfaces. Introduction of a spatially correlated disorder with a spectrum $D(k) \sim 1/|k|^{2\rho}$ (i.e., the direct space correlations $\sim |r-r'|^{2\rho-1}$) results in $\alpha = 1/2 + 2(\rho - 1/4)/3$.² At $\rho \rightarrow 1/2$, $\alpha \rightarrow 2/3$ in accordance with values we observe behind the front. Similar large α emerges in the case of temporal correlations.² Note that the long-range interactions ($\rho \sim 1/2$) should be expected in thin films, where the electrodynamics is essentially nonlocal¹⁹ and vortices are coupled by slowly decaying Pearls forces²⁰ rather than by the exponential repulsion relevant for bulk superconductors. Therefore correlations can be a reason for the large α we obtained.

At the same time, more naturally, our experiment could be related to the directed percolation depinning model (DPD) simulating the (1+1)-dimensional interface propagating through the quenched disorder.² In this model $\alpha = 2/3$, close to our value behind the front. DPD is similar to the KPZ model with quenched disorder (QKPZ). The latter considers different scaling regimes depending on the driving force. It predicts $\alpha = 0.63$ for mainly pinned interfaces and $\alpha = 0.75$ for interfaces moving in the critical regime. There are other quenched disorder processes generating $\alpha \sim 0.7$ in the (1+1) dimension. They show a strong relevance to power-law noise driven interfaces² which could be expected accounting that

such a noise is intrinsic for the rough motion. Presently, universality classes for the quenched disorder models are not so well defined. However, we believe that the directed percolation belonging to the same class as QKPZ could be relevant to our experimental situation.

We would like to draw a special attention to the peculiar variations of D and α near $B_z=0$ (Fig. 3). They may be associated with vortices scattered ahead of the continuous flux front and defining a very tortuous B_z profile and producing the largest D . Actually, at $B_z \sim 0$ $L(\ell)$ is more noisy than that shown in Fig. 2(c). This can be related to results of the molecular-dynamic simulations²¹ showing that the dimension D increases with decreasing pinning forces. Considering that vortices at the flux front choose the easiest channels in the random potential (minimum effective pinning) the profiles at $B_z \sim 0$ should have the largest D . Further rows of vortices can be stabilized not only by pinning but also by the magnetization currents J_m localized at the front which should work as effective surface tension and reduce D . In a bulk superconductor J_m produces $\sim H_{c1}$ step in $B(x)$ at the penetration front (dB/dH effect²²). A physically similar picture is obtained if the advanced vortices are considered frozen after motion above the pinning threshold as implied by the annealed noise regime of the KPZ process ($\alpha \sim 0.5$, Ref. 2). Behind the front they are more relaxed due to interactions with close neighbors showing the critical regime of motion in the quenched disorder ($\alpha > 0.63$). In any case, a counterintuitive reduction of the roughness exponent at $B_z \sim 0$ can be understood as a compensation for the increased D preserving the scaling relation $D + \alpha = 2$. Note a difference of

our results from Ref. 13 where $\alpha = 0.64$ was reported just at the front and a change to $\alpha = 0.46$ was inferred for large scales from the kink at $C(\ell)$ that we see as an artifact of treatment.

In conclusion, it is directly observed that in an intermediate range of temperatures, between $T \sim 2/3T_c$ (when the strong thermally activated flux creep smoothes vortex patterns) and $T \sim 4.2$ K (when strong thermomagnetic avalanches severely disturb the flux distribution), the flux entry occurs through vortex avalanches with a wide range of scales. The resulting critical state shows the self-affine structure characterized by universal exponents which can be associated with the directed percolation process belonging to the universality class of the QKPZ model. Typical for the films, long-range interactions between vortices may be an important factor influencing the flux dynamics. The exponents at the flux front and behind it are different revealing different scaling regimes. We stress here that all the exponents are obtained by the regular statistical treatment of the experimental data and are not based on any model. These exponents are similar to those observed in other fractal structures. The results show that not only the flux front but all induction profiles carry the fingerprints of the SOC in the vortex system indicating that our approach is a useful tool for studying the flux fractality in superconductors.

The work was supported by the U.S. Department of Energy, Office of Science under Contract No. W-31-109-ENG-38.

-
- ¹P. Bak, C. Tang, and K. Wiesenfeld, Phys. Rev. Lett. **59**, 381 (1987); Phys. Rev. A **38**, 364 (1988).
- ²T. Vicsek, *Fractal Growth Phenomena* (World Scientific, Singapore, New Jersey, 1992); A.-L. Barabasi and H.E. Stanley, *Fractal Concepts in Surface Growth* (Cambridge University Press, Cambridge, 1995); P. Meakin, *Fractals, Scaling and Growth Far from Equilibrium* (Cambridge University Press, Cambridge, 1998).
- ³M. Paczuski, S. Maslov, and P. Bak, Phys. Rev. E **53**, 414 (1996).
- ⁴C. Heiden and G.I. Rochlin, Phys. Rev. Lett. **21**, 691 (1968).
- ⁵S. Field, J. Witt, F. Nori, and X. Ling, Phys. Rev. Lett. **74**, 1206 (1995).
- ⁶E.R. Nowak, O.W. Taylor, L. Liu, H.M. Jaeger, and T.I. Selinder, Phys. Rev. B **55**, 11 702 (1997).
- ⁷K. Behnia, C. Capan, D. Maily, and B. Etienne, Phys. Rev. B **61**, R3815 (2000).
- ⁸S. Ooi, T. Shibaushi, and T. Tamegai, Physica B **284-288**, 775 (2000).
- ⁹Z. Wang and D. Shi, Phys. Rev. B **48**, 9782 (1993); Solid State Commun. **90**, 405 (1994).
- ¹⁰C.M. Aegerter, Phys. Rev. E **58**, 1438 (1998).
- ¹¹E. Bonabeau and P. Lederer, Phys. Rev. B **52**, 494 (1995); Physica C **256**, 365 (1996).
- ¹²R. Mulet, R. Cruz, and E. Altshuler, Phys. Rev. B **63**, 094501 (2001).
- ¹³R. Surdeanu, R.J. Wijngaarden, E. Visser, J.M. Huijbregste, J.H. Rector, B. Dam, and R. Griessen, Phys. Rev. Lett. **83**, 2054 (1999).
- ¹⁴V. Vlasko-Vlasov, G.W. Crabtree, U. Welp, and V.I. Nikitenko, in *Physics and Materials Science of Vortex States*, Vol. 356 of *NATO Advanced Study Institute, Series E: Applied Sciences*, edited by R. Kossowsky *et al.* (Kluwer Academic, Dordrecht, 1999), p. 205.
- ¹⁵V. Bujok, P. Brull, J. Boneberg, S. Herminghaus, and P. Leiderer, Appl. Phys. Lett. **63**, 412 (1993).
- ¹⁶J.M. Lopez and J. Schmittbuhl, Phys. Rev. E **57**, 6405 (1998).
- ¹⁷J.J. Ramasco, J.M. Lopez, and M.A. Rodriguez, Phys. Rev. Lett. **84**, 2199 (2000).
- ¹⁸J. Soriano, J.J. Ramasco, M.A. Rodriguez, A. Hernandez-Machado, and J. Ortin, Phys. Rev. Lett. **89**, 026102 (2002); J. Soriano, J. Ortin, and A. Hernandez-Machado, Phys. Rev. E **66**, 031603 (2002).
- ¹⁹A. Gurevich, Int. J. Mod. Phys. B **9**, 1045 (1995).
- ²⁰J. Pearl, Appl. Phys. Lett. **5**, 65 (1964).
- ²¹C.J. Olson, C. Reichhardt, and F. Nori, Phys. Rev. Lett. **80**, 2197 (1998).
- ²²M.A.R. LeBlanc, S.X. Wang, D. LeBlanc, M. Krzywinski, and J. Meng, Phys. Rev. B **52**, 12 895 (1995).